Supporting Information for

Deriving Paired Fe Sites on N-Doped Carbon from Fe(III)-Tetrapyridinylporphyrin-Modified ZIF-8: Robust Electrocatalysts for Air Electrodes in Zinc-Air Batteries

Guiyuan Yang,[a] Fangyuan Hu,[a] Li-Li Cui,[a] Meihong Fan,[a] Xin Ge,[b] Xingquan He*[,a] Wei Zhang*[,b] Tewodros Asefa*[,c]

[a] School of Chemistry and Environmental Engineering, Changchun University of Science and Technology; 7089 Weixing Road, Changchun 130022, P. R. China

[b] Key Laboratory of Automobile Materials MOE, School of Materials Science & Engineering, Jilin Provincial International Cooperation Key Laboratory of High-Efficiency Clean Energy Materials, and Electron Microscopy Center, and International Center of Future Science, Jilin University, 2699 Qianjin Street, Changchun 130012, P. R. China

[c] Department of Chemistry and Chemical Biology & Department of Chemical and Biochemical Engineering, Rutgers, The State University of New Jersey, 610 taylor Road, Piscataway, New Jersey 08854, USA

* Corresponding authors' e-mails: hexingquan@hotmail.com (X. He); weizhang@jlu.edu.cn (W. Zhang); tasefa@chem.rutgers.edu (T. Asefa)

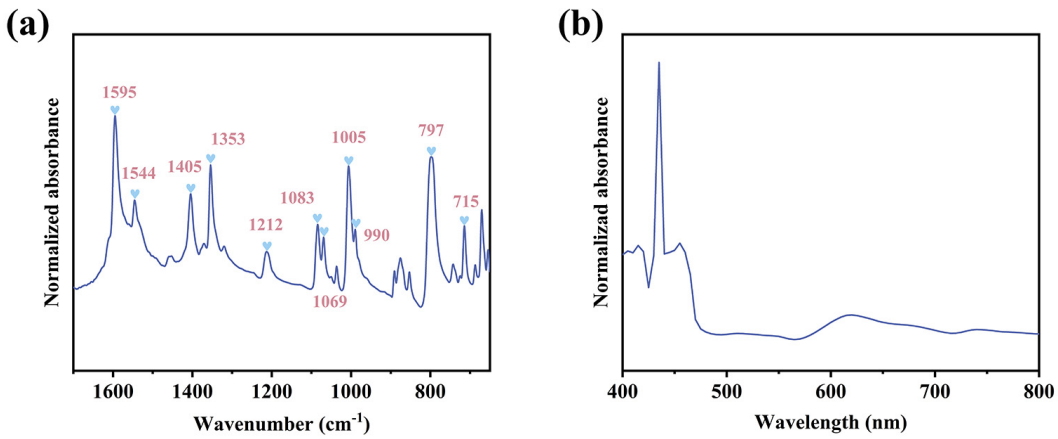

Figure S1. (a) Attenuated total reflectance Fourier-transform infrared (FTIR) spectrum of powder FeTPyP and (b) UV-Vis absorption spectrum of FeTPyP dissolved in *N*,*N*-dimethylformamide. The FT-IR spectrum of FeTPyP exhibits typical vibration peaks attributable to the Fe(III)-modified 5,10,15,20-tetrakis(4-pyridyl)porphyrin, and the UV-Vis spectrum of FeTPyP shows the typical absorption peaks of the Fe(III)-modified 5,10,15,20-tetrakis(4-pyridyl)porphyrin at 435 nm (a B band) and 620 nm (a Q band), as reported previously.[1]

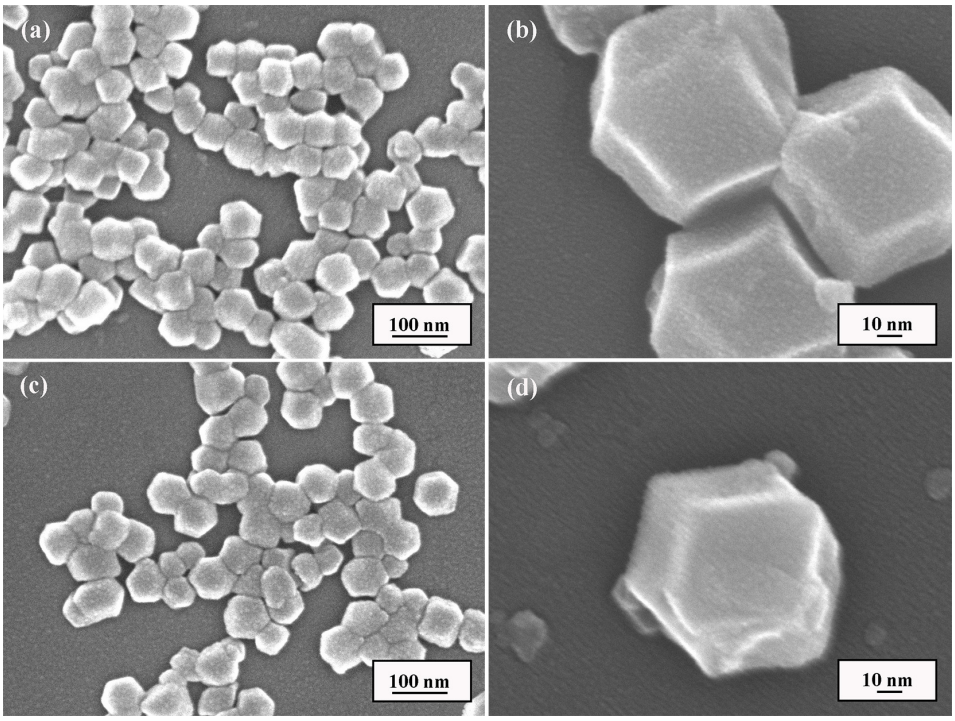

Figure S2. SEM images of (a,b) ZIF-8 and (c,d) ZIF-8/FeTPyP.

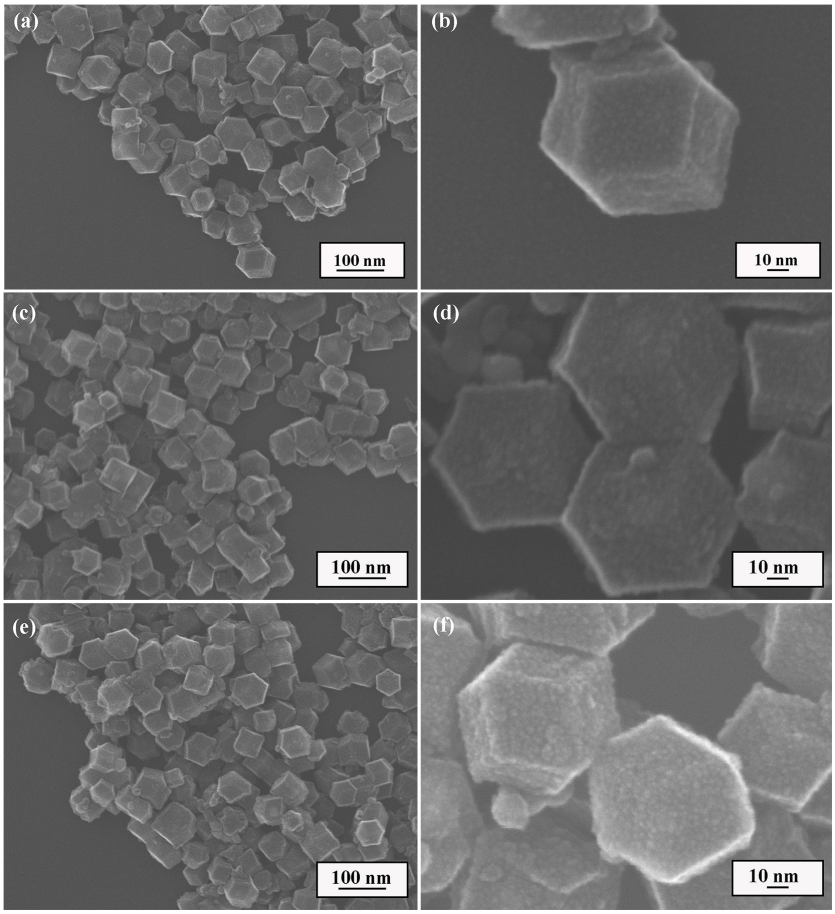

Figure S3. SEM images of (a,b) Fe_2-N-C-900, (c,d) ZIF-8/FeTPP-900, and (e,f) N-C-900.

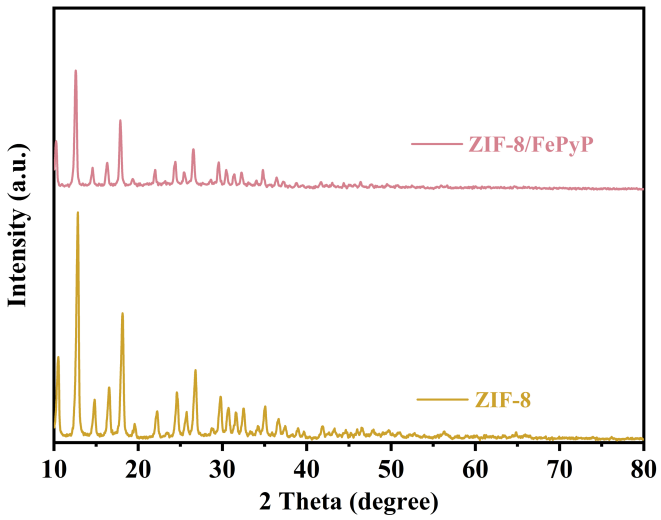

Figure S4. X-ray diffraction patterns of ZIF-8 and ZIF-8/FeTPyP. The XRD patterns show that the modification of ZIF-8 with FeTPyP results in no distinct change in the XRD pattern of ZIF-8. In other words, the modification of ZIF-8 with FeTPyP does not change the crystal structure of ZIF-8.

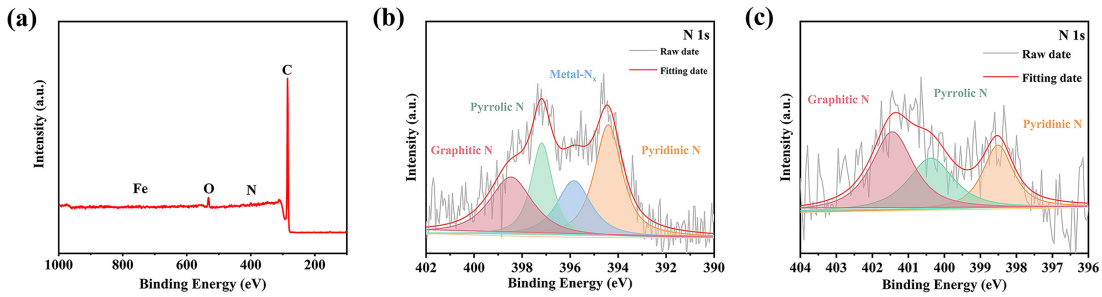

Figure S5. (a) XPS survey spectrum of Fe_2-N-C-900 and (b,c) high-resolution XPS spectra of N 1s of ZIF-8/FeTPP-900 and N-C-900, respectively.

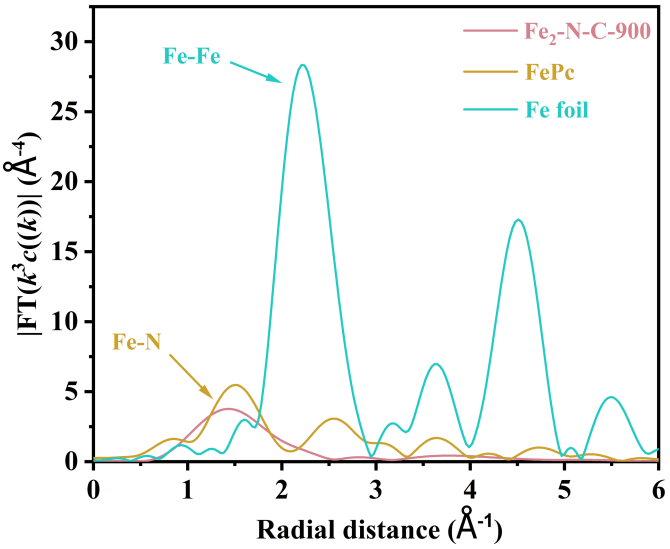

Figure S6. Fourier transform (FT) profiles of Fe K-edge EXAFS oscillations of planar-like Fe_2N_6 structure. Those for Fe foil and FePc are also obtained and included for reference.

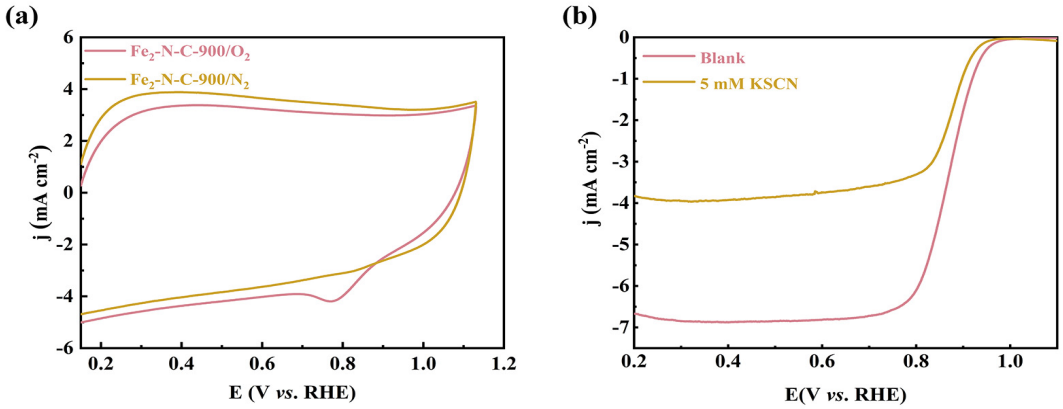

Figure S7. (a) CV curves of Fe_2-N-C-900 and commercial Pt/C in O_2- and N_2-saturated alkaline electrolyte (0.1 M KOH) at 100 mV s^{-1}. (b) LSV curves of Fe_2-N-C-900 and Pt/C in O_2-saturated KOH solution (0.1 M) before and after addition of KSCN into the solution, respectively.

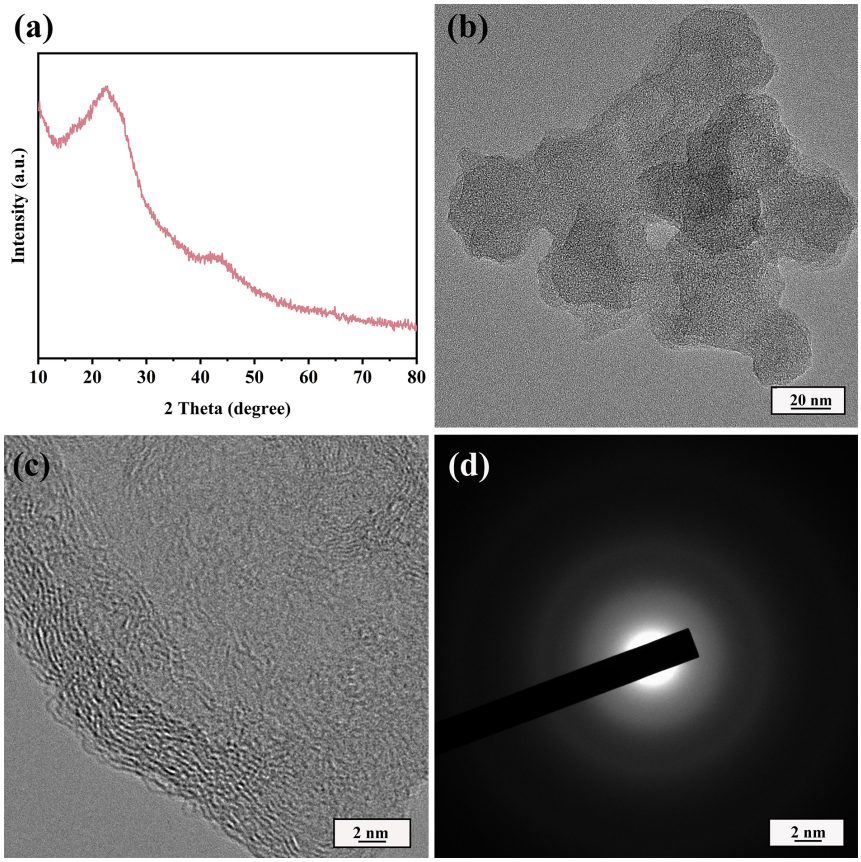

Figure S8. (a) The XRD pattern, (b) TEM image, (c) high resolution TEM image, and (d) SAED image of Fe_2-N-C-900 after the stability test for ORR.

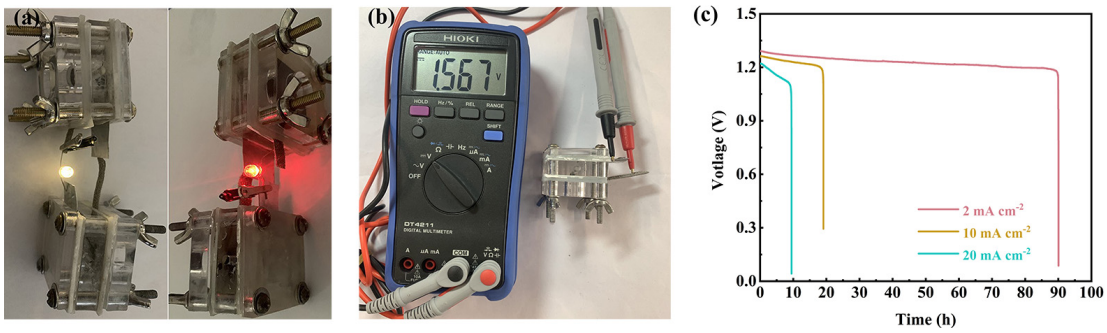

Figure S9. (a) LEDs powered by two Fe_2-N-C-900-based ZABs connected in series are displayed. (b) Photographs of a ZAB displaying its measured open-circuit voltage of 1.567 V. (c) V Galvanostatic discharge voltage versus time curves of ZABs containing Fe_2-N-C-900 as electrocatalyst at the cathode at current densities of 2, 10, and 20 mA cm^{-2}.

Table S1. Comparison of the porosity of the different materials synthesized and studied.

Materials/Catalysts	SSA ($m^2 g^{-1}$)	Pore volume ($cm^3 g^{-1}$)
Fe_2-N-C-900	697	2.483
ZIF-8/FeTPP-900	413	1.724
N-C-900	493	0.374

Table S2. Relative amounts of the elements present on the surfaces of the materials, as determined by XPS analysis.

Materials/Catalysts	Fe	C	N	O
Fe_2-N-C-900	0.53	90.7	5.06	3.31
ZIF-8/FeTPP-900	0.57	90.07	3.55	5.2
N-C-900	--	92.82	2.05	3.86

Table S3. The types and amounts of surface N species on the materials, as determined by XPS.

Materials/Catalysts	N (at. %)	Pyridinic N (at. %)	Metal-N (at. %)	Pyrrolic N (at. %)	Graphitic N (at. %)
Fe_2-N-C-900	5.06	23.07	24.66	19.19	33.08
ZIF-8/FeTPP-900	3.55	22.33	21.20	23.81	32.66
N-C-900	2.05	25.53	--	31.10	43.37

Table S4. EXAFS fitting parameters at the Fe K-edge for various materials (S_0^2 = 0.719).

Materials	Shell	CN^a	R(Å)^b	σ^2(Å^2)^c	ΔE_0(eV)^d	R factor
Fe foil	Fe-Fe	8*	2.47±0.01	0.0042±0.0007	7.2	0.0016
	Fe-Fe	6*	2.86±0.01	0.0055±0.0012		
FePc	Fe-N	3.8±0.7	2.00±0.01	0.0113±0.0021	6.2	0.0086
	Fe-C	6.0±1.1	3.00±0.01	0.0063±0.0014		
Fe_2-N-C-900	Fe-N	4.3±0.9	1.98±0.02	0.0101±0.0043	3.5	0.0192

Table S5. Electrocatalytic activities for ORR over the different materials in 0.1 M KOH electrolyte.

Materials/Catalysts	E_{oneset} (V)	$E_{1/2}$ (V)	j_L [mA cm^{-2}]
Fe_2-N-C-900	0.990	0.869	-6.67
ZIF-8/FeTPP-900	0.958	0.851	-5.33
N-C-900	0.932	0.805	-5.18
Pt/C	1.001	0.850	-5.65

Table S6. Comparison of E_{onset} and $E_{1/2}$ required by ORR in 0.1 M KOH solution over Fe-N-C-900 versus those of various non-noble metal catalysts recently reported in the literature.

Materials/Catalysts	E_{onset} (V)	$E_{1/2}$ (V)	Electrolytes	References
FeN_4SAs/NPC	0.972	0.885	1 M KOH	2
Fe/N-G-SAC	0.988	0.890	1 M KOH	3
Fe-N-C HNSs	1.06	0.87	0.1 M KOH	4
Fe-N-C/N-OMC	1.08	0.93	0.1 M KOH	5
Fe-IICSAC	1.01	0.908	0.1 M KOH	6
Fe-N/C-1/30	1.04	0.895	0.1 M KOH	7
FeN_2/NOMC	0.98	0.89	0.1 M KOH	8
FeN_3OS	1.01	0.874	0.1 M KOH	9
OAC	0.98	0.854	0.1 M KOH	10
FeNC-F3	0.988	0.858	0.1 M KOH	11
L-FeNC	0.99	0.89	0.1 M KOH	12
3DOM Fe-N-C	0.997	0.875	0.1 M KOH	13
Fe SAs/N-C	1.01	0.91	0.1 M KOH	14
Fe-N-C/Rgo	0.99	0.90	0.1 M KOH	15
Fe-SA/Micro-C	1.05	0.926	0.1 M KOH	16
Fe-NCNWs	1.02	0.91	0.1 M KOH	17
Fe/NSC^N (1^N)	1.14	0.87	0.1 M KOH	18
meso-Fe-N-C	0.998	0.846	0.1 M KOH	19
ISG Fe-N-C	1.02	0.91	0.1 M KOH	20
Fe-N/GNs	1.01	0.903	0.1 M KOH	21
Fe_2-N-C-900	**0.990**	**0.869**	**0.1 M KOH**	**This work**

Table S7. The values of C_{dl} and R_{ct} of different catalysts obtained from the equivalent circuit model with electrochemical impedance spectroscopy (EIS).

Materials/Catalysts	C_{dl} (mF cm^{-2})	R_{ct} (Ω)
Fe_2-N-C-900	14.52	307
ZIF-8/FeTPP-900	10.19	480
N-C-900	7.88	991
Pt/C	13.49	477

Table S8. Comparison of the performances of ZAB assembled using the synthesized catalyst reported herein (Fe_2-N-C-900) in this work as the air cathode with respect to ZABs containing other single-atom catalysts recently reported in the literature.

Catalysts	Electrolyte	OCV (V)	PPD (mW cm^{-2})	References
Fe/NCNF	6 M KOH	1.54	146	[22]
Fe_1/NC	6 M KOH	1.45	164	[23]
3D SAFe	6 M KOH	1.47	156	[24]
ISG Fe-N-C	6 M KOH	1.45	155	[20]
Fe-SASCs	6 M KOH	1.47	78	[25]
FeSA/ N-PSCS	6 M KOH	1.45	164.5	[26]
FePc-c–NG-10	6 M KOH	1.45	141	[27]
3DOM Fe-N-C-900	6 M KOH	1.47	175.9	[28]
Fe-SA/NCS	6 M KOH	1.53	141.6	[29]
FeSA/NSC	6 M KOH	1.501	159	[30]
CPANI-TA-Fe-SA-NC	6 M KOH	1.44	136	[31]
Fe-N-C	6 M KOH	1.453	131	[32]
SAC-FeN-WPC	6 M KOH	1.32	70.2	[33]
Fe/Z_8-E-C	6 M KOH	1.58	157.8	[34]
Fe-N-C/RGO	6 M KOH	1.52	107.12	[35]
Fe-N-C-700	6 M KOH	1.425	70	[36]
Fe/N-G-800	6 M KOH	1.56	136	[37]
Fe_2-N-C-900	**6 M KOH**	**1.567**	**166.3**	**This work**

References

1 K. Tomita, N. Shioya, T. Shimoaka, M. Wakioka and T. Hasegawa, Control of supramolecular organizations by coordination bonding in tetrapyridylporphyrin thin films, *Chem. Comm.*, 2022, **58**, 2116-2119.

2 J. C. Li, Y. Meng, R. Ma, H. Hu, S. Zhao, Y. Zhu, P. X. Hou and C. Liu, Ionothermal-Transformation Strategy to Synthesize Hierarchically Tubular Porous Single-Iron-Atom Catalysts for High-Performance Zinc-Air Batteries, *ACS Appl Mater Interfaces*, 2021, **13**, 58576-58584.

3 M. Xiao, Z. Xing, Z. Jin, C. Liu, J. Ge, J. Zhu, Y. Wang, X. Zhao and Z. Chen, Preferentially engineering FeN(4) edge sites onto graphitic nanosheets for highly active and durable oxygen electrocatalysis in rechargeable Zn-Air batteries, *Adv. Mater.*, 2020, **32**, e2004900.

4 Y. Chen, Z. Li, Y. Zhu, D. Sun, X. Liu, L. Xu and Y. Tang, Atomic Fe Dispersed on N-Doped Carbon Hollow Nanospheres for High-Efficiency Electrocatalytic Oxygen Reduction, *Adv Mater*, 2019, **31**, e1806312.

5 J. Han, H. Bao, J.-Q. Wang, L. Zheng, S. Sun, Z. L. Wang and C. Sun, 3D N-doped ordered mesoporous carbon supported single-atom Fe-N-C catalysts with superior performance for oxygen reduction reaction and zinc-air battery, *Appl. Catal. B*, 2021, **280**, 119411.

6 S. Ding, Z. Lyu, H. Zhong, D. Liu, E. Sarnello, L. Fang, M. Xu, M. H. Engelhard, H. Tian, T. Li, X. Pan, S. P. Beckman, S. Feng, D. Du, J. C. Li, M. Shao and Y. Lin, An Ion-Imprinting Derived Strategy to Synthesize Single-Atom Iron Electrocatalysts for Oxygen Reduction, *Small*, 2021, **17**, e2004454.

7 W. Wei, X. Shi, P. Gao, S. Wang, W. Hu, X. Zhao, Y. Ni, X. Xu, Y. Xu, W. Yan, H. Ji and M. Cao, Well-elaborated, mechanochemically synthesized Fe-TPP@ZIF precursors (Fe-TPP=tetraphenylporphine iron) to atomically dispersed iron-nitrogen species for oxygen reduction reaction and Zn-air batteries, *Nano Energy*, 2018, **52**, 29-37.

8 H. Shen, E. Gracia-Espino, J. Ma, H. Tang, X. Mamat, T. Wagberg, G. Hu and S. Guo, Atomically FeN2 moieties dispersed on mesoporous carbon: A new atomic catalyst for efficient oxygen reduction catalysis, *Nano Energy*, 2017, **35**, 9-16.

9 L. Yu, Y. Li and Y. Ruan, Dynamic control of sacrificial bond transformation in the Fe-N-C single-atom catalyst for molecular oxygen reduction, *Angew. Chem. Int. Ed.*, 2021, **60**, 25296-25301.

10 L. Deng, L. Qiu, R. Hu, L. Yao, Z. Zheng, X. Ren, Y. Li and C. He, Restricted diffusion preparation of fully-exposed Fe single-atom catalyst on carbon nanospheres for efficient oxygen reduction reaction, *Appl. Catal. B*, 2022, **305**, 121058.

11 C. Shao, L. Wu, Y. Wang, K. Qu, H. Chu, L. Sun, J. Ye, B. Li and X. Wang, An open superstructure of hydrangea-like carbon with highly accessible Fe-N_4 active sites for enhanced oxygen reduction reaction, *Chem. Eng. J.*, 2022, **429**, 132307.

12 X. Jiang, J. Chen, F. Lyu, C. Cheng, Q. Zhong, X. Wang, A. Mahsud, L. Zhang and Q.

Zhang, In situ surface-confined fabrication of single atomic Fe-N_4 on N-doped carbon nanoleaves for oxygen reduction reaction, *J. Energy Chem.*, 2021, **59**, 482-491.

13 F. Xiao, G.-L. Xu, C.-J. Sun, M. Xu, W. Wen, Q. Wang, M. Gu, S. Zhu, Y. Li, Z. Wei, X. Pan, J. Wang, K. Amine and M. Shao, Nitrogen-coordinated single iron atom catalysts derived from metal organic frameworks for oxygen reduction reaction, *Nano Energy*, 2019, **61**, 60-68.

14 Z. Yang, Y. Wang, M. Zhu, Z. Li, W. Chen, W. Wei, T. Yuan, Y. Qu, Q. Xu, C. Zhao, X. Wang, P. Li, Y. Li, Y. Wu and Y. Li, Boosting Oxygen Reduction Catalysis with Fe–N4 Sites Decorated Porous Carbons toward Fuel Cells, *ACS Catalysis*, 2019, **9**, 2158-2163.

15 L. Li, Y.-J. Chen, H.-R. Xing, N. Li, J.-W. Xia, X.-Y. Qian, H. Xu, W.-Z. Li, F.-X. Yin, G.-Y. He and H.-Q. Chen, Single-atom Fe-N5 catalyst for high-performance zinc-air batteries, *Nano Research*, 2022, **15**, 8056-8064.

16 X. Wang, H. Zhu, C. Yang, J. Lu, L. Zheng and H.-P. Liang, Mesoporous carbon promoting the efficiency and stability of single atomic electrocatalysts for oxygen reduction reaction, *Carbon*, 2022, **191**, 393-402.

17 J.-C. Li, F. Xiao, H. Zhong, T. Li, M. Xu, L. Ma, M. Cheng, D. Liu, S. Feng, Q. Shi, H.-M. Cheng, C. Liu, D. Du, S. P. Beckman, X. Pan, Y. Lin and M. Shao, Secondary-Atom-Assisted Synthesis of Single Iron Atoms Anchored on N-Doped Carbon Nanowires for Oxygen Reduction Reaction, *ACS Catalysis*, 2019, **9**, 5929-5934.

18 X. Zhang, L. Truong-Phuoc, X. Liao, G. Tuci, E. Fonda, V. Papaefthymiou, S. Zafeiratos, G. Giambastiani, S. Pronkin and C. Pham-Huu, An Open Gate for High-Density Metal Ions in N-Doped Carbon Networks: Powering Fe–N–C Catalyst Efficiency in the Oxygen Reduction Reaction, *ACS Catalysis*, 2021, **11**, 8915-8928.

19 Y. Zhou, Y. Yu, D. Ma, A. C. Foucher, L. Xiong, J. Zhang, E. A. Stach, Q. Yue and Y. Kang, Atomic Fe Dispersed Hierarchical Mesoporous Fe–N–C Nanostructures for an Efficient Oxygen Reduction Reaction, *ACS Catalysis*, 2020, **11**, 74-81.

20 Y. Wang, Q. Li, L.-c. Zhang, Y. Wu, H. Chen, T. Li, M. Xu and S.-J. Bao, A gel-limiting strategy for large-scale fabrication of Fe-N-C single-atom ORR catalysts, *J. Mater. Chem. A*, 2021, **9**, 7137-7142.

21 D. Liu, J. C. Li, S. Ding, Z. Lyu, S. Feng, H. Tian, C. Huyan, M. Xu, T. Li, D. Du, P. Liu, M. Shao and Y. Lin, 2D Single-Atom Catalyst with Optimized Iron Sites Produced by Thermal Melting of Metal–Organic Frameworks for Oxygen Reduction Reaction, *Small Methods*, 2020, **4**.

22 H. Liu, C. Wang, X. Ai, B. Wang, Y. Bian, G. Wang, Y. Wang, Z. Hu and Z. Zhang, Stabilizing iron single atoms with electrospun hollow carbon nanofibers as self-standing air-electrodes for long-time Zn-air batteries, *J. Colloid Interface Sci.*, 2023, **651**, 525-533.

23 L. Cao, X. Shi, Y. Li, X. Wang, L. Zheng and H.-P. Liang, Isolation anchoring strategy for in situ synthesis of iron single-atom catalysts towards long-term rechargeable zinc-air battery, *Carbon*, 2022, **199**, 387-394.

24 L. J. W. M.S. Liu, L. Zhang, Y. Zhao, K. Chen, Y.X. Li, X. Yang, In-situ silica xerogel assisted facile synthesis of Fe-N-C catalysts with dense Fe-N_x active sites for efficient oxygen reduction, *Small*, 2021, **18**, 202104934.

25 W. Ye, S. Chen, Y. Lin, L. Yang, S. Chen, X. Zheng, Z. Qi, C. Wang, R. Long, M. Chen, J. Zhu, P. Gao, L. Song, J. Jiang and Y. Xiong, Precisely tuning the number of Fe atoms in clusters on N-doped carbon toward acidic oxygen reduction reaction, *Chem. Comm.*, 2019, **5**, 2865-2878.

26 M. Shen, J. Liu, J. Li, C. Duan, C. Xiong, W. Zhao, L. Dai, Q. Wang, H. Yang and Y. Ni, Breaking the N-limitation with N-enriched porous submicron carbon spheres anchored Fe single-atom catalyst for superior oxygen reduction reaction and Zn-air batteries, *Energy Stor. Mater.*, 2023, **59**.

27 Y. Wu, X. Wang, B. Tian, W. Shuang, Z. Bai and L. Yang, Optimizing reaction intermediate adsorption by engineering the coordination structure of single-atom Fe-N_5-C electrocatalysts for efficient oxygen reduction, *Inorg. Chem. Front.*, 2023, **10**, 4209-4220.

28 X. Zhang, X. Han, Z. Jiang, J. Xu, L. Chen, Y. Xue, A. Nie, Z. Xie, Q. Kuang and L. Zheng, Atomically dispersed hierarchically ordered porous Fe-N-C electrocatalyst for high performance electrocatalytic oxygen reduction in Zn-Air battery, *Nano Energy*, 2020, **71**, 104547.

29 X. Wang, C. Yang, X. Wang, H. Zhu, L. Cao, A. Chen, L. Gu, Q. Zhang, L. Zheng and H.-P. Liang, Green synthesis of a highly efficient and stable single-atom Iron catalyst anchored on nitrogen-doped carbon nanorods for the oxygen reduction reaction, *ACS Sustain. Chem. Eng.*, 2020, **9**, 137-146.

30 X. Liu, X. Zhai, W. Sheng, J. Tu, Z. Zhao, Y. Shi, C. Xu, G. Ge and X. Jia, Isolated single iron atoms anchored on a N, S-codoped hierarchically ordered porous carbon framework for highly efficient oxygen reduction, *J. Mater. Chem. A*, 2021, **9**, 10110-10119.

31 H. Li, K. Du, C. Xiang, P. An, X. Shu, Y. Dang, C. Wu, J. Wang, W. Du, J. Zhang, S. Li, H. Tian, S. Wang and H. Xia, Controlled chelation between tannic acid and Fe precursors to obtain N, S co-doped carbon with high density Fe-single atom-nanoclusters for highly efficient oxygen reduction reaction in Zn–air batteries, *J. Mater. Chem. A*, 2020, **8**, 17136-17149.

32 H. Xu, L. Xiao, P. Yang, X. Lu, L. Liu, D. Wang, J. Zhang and M. An, Solvent environment engineering to synthesize Fe N C nanocubes with densely Fe-N_x sites as oxygen reduction catalysts for Zn-air battery, *J. Colloid Interface Sci.*, 2023, **638**, 242-251.

33 L. Zhong, C. Jiang, M. Zheng, X. Peng, T. Liu, S. Xi, X. Chi, Q. Zhang, L. Gu, S. Zhang, G. Shi, L. Zhang, K. Wu, Z. Chen, T. Li, M. Dahbi, J. Alami, K. Amine and J. Lu, Wood carbon based single-atom catalyst for rechargeable Zn–air batteries, *ACS Energy Lett.*, 2021, **6**, 3624-3633.

34 Y. Jia, F. Zhang, Q. Liu, J. Yang, J. Xian, Y. Sun, Y. Li and G. Li, Single-atomic Fe anchored on hierarchically porous carbon frame for efficient oxygen reduction performance, *Chinese Chem. Lett.*, 2022, **33**, 1070-1073.

35 L. Li, Y.-J. Chen, H.-R. Xing, N. Li, J.-W. Xia, X.-Y. Qian, H. Xu, W.-Z. Li, F.-X. Yin, G.-Y. He and H.-Q. Chen, Single-atom Fe-N_5 catalyst for high-performance zinc-air batteries, *Nano Res.*, 2022, **15**, 8056-8064.

36 T. Chen, J. Wu, C. Zhu, Z. Liu, W. Zhou, C. Zhu, C. Guan and G. Fang, Rational design of iron single atom anchored on nitrogen doped carbon as a high-performance electrocatalyst for all-solid-state flexible zinc-air batteries, *Chem. Eng. J.*, 2021, **405**, 125956.

37 C. Xu, Y. Si, B. Hu, X. Xu, B. Hu, Y. Jiang, H. Chen, C. Guo, H. Li and C. Chen, Promoting oxygen reduction via crafting bridge-bonded oxygen ligands on a single-atom iron catalyst, *Inorg. Chem. Front.*, 2022, **9**, 3306-3318.